J Supercond Nov Magn (2016) 29:1525–1532
DOI 10.1007/s10948-016-3423-4

ORIGINAL PAPER

Structural, Morphological, Optical and Magnetic Properties of Al-Doped $CoFe_2O_4$ Nanoparticles Prepared by Sol–Gel Auto-Combustion Method

Sara Ansari[1] · Hadi Arabi[2] · Seyyed Mojtaba Alavi Sadr (Zareii)[3]

Received: 4 December 2015 / Accepted: 20 January 2016 / Published online: 6 February 2016
© Springer Science+Business Media New York 2016

Abstract $CoFe_{2-x}Al_xO_4$ ($x = 0.0, 0.5, 1.0$, and 1.5) ferrite nanoparticles have been synthesized by the sol–gel auto-combustion method. The effect of non-magnetic Al content on their structural, morphological, optical, and magnetic properties was also investigated. X-ray diffraction (XRD) diffraction analysis was applied and indicated that the synthesized nanopowders of samples with $x < 1.5$ and calcined at 800 °C have single-phase spinel structure. It has shown also by increasing Al content, the particle size, lattice parameter, unit cell volume, coercivity, anisotropy constant, and magnetization decrease, while the energy band gap increases. The size of particles was measured by TEM being in the range of 65–75 nm (for $x = 0.0$) and 9–10 nm (for $x = 1.0$). For sample with $x = 1.5$, the minimum calcination temperature for obtaining a single-phase spinel structure was 1000 °C. By increasing the calcination temperature from 1000 to 1100 °C, the mean crystallite size and crystallinity increase, while the lattice parameter, coercivity, anisotropy constant, and magnetization decrease. The average grain size evaluated by SEM analysis was found to be $\tilde{9}1$ and 166 nm for samples calcined at 1000 and 1100 °C, respectively.

✉ Hadi Arabi
arabi-h@um.ac.ir

[1] Department of Physics, Faculty of Science, University of Birjand, Birjand, Iran

[2] Department of Physics, Faculty of Science, Ferdowsi University of Mashhad, Mashhad, Iran

[3] Department of Basic Sciences, Birjand University of Technology, Birjand, Iran

Keywords Sol–gel · Al substitution · Co ferrite · Structural properties · Band gap · Magnetic properties

1 Introduction

The spinel ferrites are commercially important materials in industry and research because of their excellent electrical and magnetic properties [1]. They have the chemical formula $(M^{2+}_{1-\lambda}Fe^{3+}_{\lambda})\left[M^{2+}_{\lambda}Fe^{3+}_{2-\lambda}\right]O_4$ where parentheses and square brackets denote cation sites of tetrahedral (A) and octahedral [B] coordination, respectively. M is a divalent metal cation, and λ (degree of inversion) is defined as the fraction of the (A) sites occupied by trivalent cations and its value depends on the preparation method [1, 2]. Among them, bulk cobalt ferrite ($CoFe_2O_4$) possess high coercivity and curie temperature, high chemical stability, high electrical resistance with low eddy current, large crystalline anisotropy, significant mechanical hardness, as well as moderate saturation magnetization (80 emu/g) [3–5]. The magnetic and electrical properties of $CoFe_2O_4$ nanoparticles are much different than those of the bulk form. Therefore, their nanoparticles have been investigated for applications in magneto optical recording, high-density storage media, magnetic sensors, actuators, magnetic catalysis, targeted drug delivery, and ferrofluids [6–9]. The properties of ferrite nanoparticles are influenced by their composition and microstructure which are sensitive to the preparation method [10] and the amount of substitution. In the past years, several methods have been used for the preparation of cobalt ferrite nanoparticles. Among them, the sol–gel auto-combustion method offers to be significant in saving time and energy consumption relative to the traditional methods because of its simplicity, low temperatures for

Content courtesy of Springer Nature, terms of use apply. Rights reserved.

synthesis, and obtaining more homogeneous nanoparticles [7–13]. It is known that the magnetic superexchange interaction and anisotropy in the spinel ferrites can be changed by cation substitution [14]. Therefore, substitution of non-magnetic Al^{+3} ions in cobalt ferrite can modify its magnetic properties [7]. In fact, Al substituted cobalt ferrite is a soft ferrite with a low magnetic coercivity, high resistivity, low dielectric constant, and negligible eddy current which make it suitable to be used at high frequencies as microwave absorbers and also as an excellent core material for power transformers in electric and telecommunication applications [4, 15]. However, there are very few detailed studies on Al-substituted cobalt ferrite [16]. Since high magnetic anisotropy of cobalt ferrite is mainly attributed to Co^{+2} ions occupying [B] sites [14], with substitution of Al for Fe, we will expect to improve the high frequency features of $CoFe_{2-x}Al_xO_4$ nanopowders while keeping high enough magnetic anisotropy. Moreover, replacement of non-magnetic Al^{+3} ion in some cases causes an increase in saturation magnetization. For example, Mozaffari et al. [13] observed such behavior for $NiFe_{2-x}Al_xO_4$ ($x = 1.5$) nanoparticles. Similar behavior may also occur in nanoferrite $CoFe_{2-x}Al_xO_4$ with $x = 1.5$, although there is no report on its synthesis so far.

Accordingly, in this paper, the synthesis of $CoFe_{2-x}Al_xO_4$ ($x = 0.0, 0.5, 1.0$, and 1.5) nanopowders has been performed by the auto-combustion sol–gel technique and structural, morphological, optical, and magnetic characterizations of them were investigated.

2 Experimental Details

For preparation of $CoFe_{2-x}Al_xO_4$ nanoferrites using sol–gel auto-combustion method, stoichiometric amounts of $Co(NO_3)_2.6H_2O$, $Fe(NO_3)_3.9H_2O$, and $Al(NO_3)_3.9H_2O$ aqueous solutions were mixed with aqueous solutions of citric acid ($C_6H_8O_7.H_2O$). The molar ratio of total metal ions to citric acid was kept as 1:3. The ammonia solution was used to adjust pH = 7, and the solution was refluxed for 4 h at 100 °C. Then, the resulting sol were heated at 80 °C for 4 h with magnetic stirring to remove the presence of water in the sol. The obtained gels were dried at 220 °C for 1 h at an oven, and subsequently, the as-prepared powders of $CoFe_{2-x}Al_xO_4$ ($x = 0, 0.5$, and 1) were calcined at 800 °C and those of $CoFe_{0.5}Al_{1.5}O_4$ were calcined at 800, 900, 1000, and 1100 °C for 2 h. Thermal analysis was carried out using thermogravimetery (TG) and derivative thermogravimetery (DTG) (model: 50 Shimadzu, Japan) in air with a heating rate of 10 °C/min. X-ray diffraction (XRD) analysis of the samples was investigated with a X'Pert PRO PANalytical system using Cu-K_α radiation ($\lambda = 1.540598$ Å). The morphology and microstructure of the nanopowders were observed both with scanning electron microscopy (SEM; model: Hitachi S9160) and transmission electron microscopy (TEM; model: LEO912AB). The optical absorption measurements of nanoferrites were recorded using a UV–visible spectrophotometer (model: Agilent 8453) to calculate the optical band gap. The room temperature magnetic properties of the samples were studied by a vibrating sample magnetometer (VSM; model: Lake Shore 7400).

3 Results and Discussion

3.1 Thermal Analysis

The structural analyses of Al-doped cobalt and nickel ferrites show that as Al content increases, the required calcination temperature to get a single-phase composition increases. As an example, TG and DTG curves of $CoFe_{2-x}Al_xO_4$ ($x = 1.0$) gel are presented in Fig. 1. The TG curve shows that thermal decomposition of the precursor is taking place through two well-defined steps. Since in dried gel, the hydroxyl group, carboxyl group, and nitrate (NO_3) ions exist [7], the first step at 60–125 °C accompanied by a weight loss of ~10 % represents the water vaporization of O–H groups (hydroxyl group). The same trends in weight loss and temperature are observed in other spinel ferrites [17]. In the second step, a large weight loss occurs at about 380 °C corresponding to a peak in DTG curve. This may be attributed to the reaction of citric acid and metal nitrates that indicates the decomposition of the carboxyl, NO_3 ions, and other organic ions presented in the gel. The total weight loss of the gel precursor was found to be $\tilde{8}1$ %. Although almost no weight loss over 450 °C indicates the completion of thermal decomposition of the gel, the formation and crystallization of the spinel phase

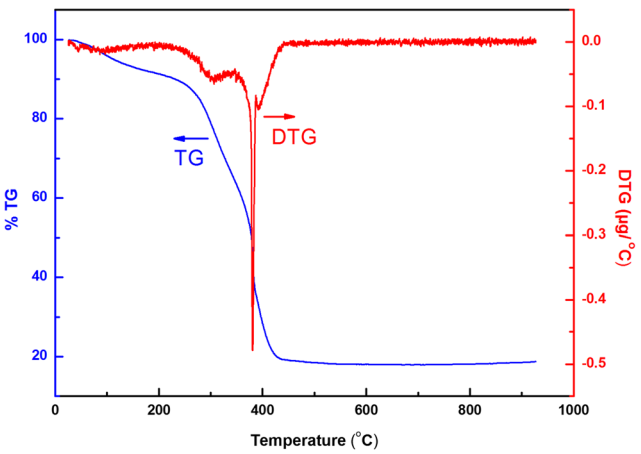

Fig. 1 TG-DTG curves of $CoFeAlO_4$ gel

Content courtesy of Springer Nature, terms of use apply. Rights reserved.

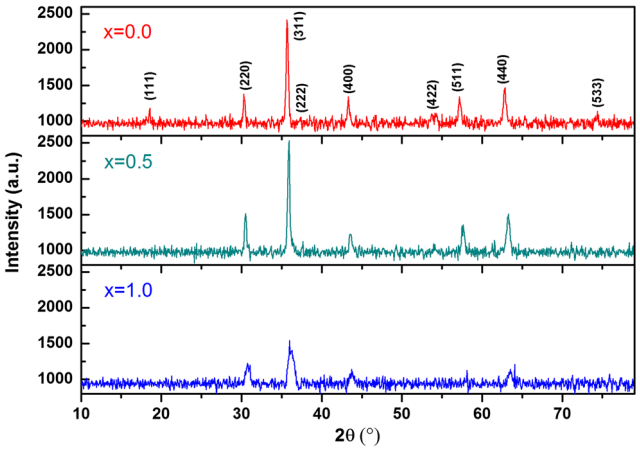

Fig. 2 XRD patterns of $CoFe_{2-x}Al_xO_4$ ($x = 0, 0.5$ and 1.0) nanopowders

may occur at higher temperatures [18]. Therefore, we have chosen 800 °C as the final calcination temperature for the samples.

3.2 Structural Characterization

Figure 2 shows the XRD patterns of $CoFe_{2-x}Al_xO_4$ ($x = 0.0, 0.5$, and 1.0) nanoparticles calcined at 800 °C. The phase identifications were performed by comparing the peak positions and intensities with those listed in the JCPDS file by using X´Pert High Score Plus program. Accordingly, all the samples are found to be a homogeneous single phase corresponding to cubic spinel structure (space group: Fd-3m, JCPDS 001-1121). The formation of spinel phase, with no extra secondary phase, indicates that the Al ions have been incorporated into the spinel lattice of these nanoparticles. However, as the Al content increases, the peak width increases which may be due to decrease in the particle size and presence of lattice strain. Moreover, with increasing Al content, the position of diffraction peaks shifts slightly towards the higher 2θ position

XRD profiles of $CoFe_{0.5}Al_{1.5}O_4$ samples calcined at 800, 900, 1000, and 1100 °C (Fig. 3) indicate the presence of Co_7Fe_3 phase (space group: Im-3m, JCPDS 050-0795) in calcined samples at 800 and 900 °C. However, the samples calcined at 1000 and 1100 °C are homogenous single phase, and all the peaks were assigned to the cubic spinel-structure. This means that the higher calcination temperatures are needed for the formation of the spinel phase in $CoFe_{0.5}Al_{1.5}O_4$ system, as also reported for $NiFe_{0.5}Al_{1.5}O_4$ [13]. Increasing the calcination temperature from 1000 to 1100 °C leads to a sharpening of the major peaks due to the growth of crystallite size of $CoFe_{0.5}Al_{1.5}O_4$ spinel powders and improved crystallization.

For a quantitative analysis of XRD test results, the average crystallite size (D) was estimated by using Scherrer and Williamson–Hall methods. According to the Scherrer formula [19]:

$$D_{\text{Scher}} = 0.9\lambda/(\beta \cos\theta) \quad (1)$$

where λ is the X-ray wavelength, θ is the angle of Bragg diffraction, β is the full-width at half maximum (FWHM) of the peaks, and D is the crystallite size. In this formula, the average crystallite size has been taken as average to all the peaks presented in Table 1. In these calculations, the contribution of peak broadening arising from the instrument was considered by using XRD profile of a pure Si sample. However, Scherrer's formula, unlike Williamson–Hall method, does not include the beak broadening arising from micro-strain [20]. The broadening effects caused by crystallite size (D_{W-H}) and micro-strain (ε) can be separated by using Williamson–Hall (W–H) and least square method [20, 21]:

$$\beta \cos\theta = 0.9\lambda/D_{W-H} + 4\varepsilon \sin\theta \quad (2)$$

From the slope and the ordinate intercept of W–H plot, i.e., $\beta\cos\theta/\lambda$ versus $4\sin\theta/\lambda$, the values of the micro-strain and average crystallite size were determined and presented in Table 1. It can be seen that the average crystallite size of the $CoFe_{2-x}Al_xO_4$ ($x = 0$, 0.5, and 1.0) samples decreases with the Al concentration. It may be due to the smaller ionic radius of Al^{+3} (0.51 Å) compared to that of Fe^{+3} (0.67 Å). Moreover, the crystal size is found to depend on the superexchange interaction strength [22]; therefore the decrease in crystallite size may also be due to weakening of superexchange interaction strength as a result of the substitution of non-magnetic Al ion. For $CoFe_{0.5}Al_{1.5}O_4$ sample, the average crystallite size increases with the increase of calcination temperature from 1000 to 1100 °C possibly due to the growth of the crystal at high temperature [23]. For all

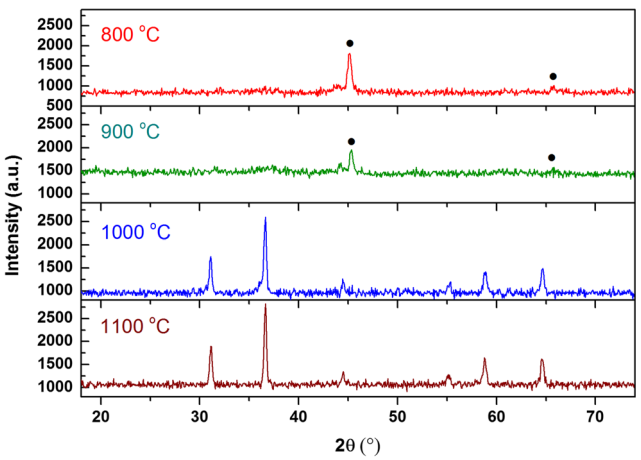

Fig. 3 XRD patterns of $CoFe_{0.5}Al_{1.5}O_4$ nanopowders calcinated at 800, 900, 1000, and 1100 °C. The *black circle symbol* denotes the typical diffraction peak of Co_7Fe_3 phase

Content courtesy of Springer Nature, terms of use apply. Rights reserved.

Table 1 The average crystallite size (D), micro-strain (ε), lattice parameter (a), unit cell volume (V), and X-ray density (d_x) of $CoFe_{2-x}Al_xO_4$ samples

Samples	D_{Scher} (nm)	D_{W-H} (nm)	ε %	a (Å)	V (Å^3)	d_x (g/cm^3)
$CoFe_2O_4$ (800 °C)	28.91	52.12	0.00164	8.3379	579.66	5.3770
$CoFe_{1.5}Al_{0.5}O_4$ (800 °C)	23.52	46.21	0.00193	8.2930	570.34	5.1285
$CoFeAlO_4$ (800 °C)	11.80	14.78	0.00177	8.2719	566.00	4.8291
$CoFe_{0.5}Al_{1.5}O_4$ (1000 °C)	25.69	27.84	0.00027	8.1432	539.99	4.7067
$CoFe_{0.5}Al_{1.5}O_4$ (1100 °C)	26.12	32.47	0.00069	8.1303	537.43	4.7292

the samples, the average crystallite sizes calculated by W–H method are found to be larger than those obtained by Scherrer formula. This can be due to the strain correction factor taken into account in case of the W–H method [23]. The lattice constant "a" was calculated using the relation [24]:

$$a = d_{hkl}\sqrt{h^2 + k^2 + l^2} \tag{3}$$

where $d_{hkl}$is the spacing between the (hkl) planes. The values of lattice constant "a," and unit cell volume "V" for each composition are calculated and tabulated in Table 1. The results show thatfor $CoFe_{2-x}Al_xO_4$ ($x = 0.0, 0.5$, and 1.0) samples, the lattice parameter decreases with increasing x which may be due to the substitution of smaller Al^{3+} ions for larger Fe^{3+} ions.

Furthermore, the lattice constant and hence unit cell size of newly developed $CoFe_{0.5}Al_{1.5}O_4$ ($x = 1.5$) ferrite powders decreases with the increase of calcination temperature from 1000 to 1100 °C. Similar behavior was also reported for $CoAl_{0.2}Fe_{1.8}O_4$ ferrite powders [15]. This can be attributed to the cation redistribution and migration of some Al^{+3} ions from tetrahedral (A) to octahedral [B] sites, as a result of increasing calcination temperature. Therefore, some Co^{2+} ions migrate from [B] to (A) sites. But the ionic radius of Al^{+3} is smaller than that of Co^{2+}, and hence, a smaller cation–anion bond for Al^{3+} in [B] sites compared to Co^{2+} in the same sites can lead to a decrease in the lattice parameter.

The X-ray density (d_x) or theoretical density of the samples (Table 1) is estimated by using the relation [24]:

$$d_x = \frac{8M}{N_a a^3} \tag{4}$$

where N_a is the Avogadro's number, M is the molecular weight, and a is the lattice constant of sample. As seen, d_x decreases with Al^{+3} content due to the decreases in the molecular weight which could not be compensated by the decreases in the unit cell volume. For $CoF_{0.5}Al_{1.5}O_4$ samples, d_x increases with calcination temperature because of a decrease in the unit cell volume.

3.3 Microstructural Characterization

TEM images of the $CoFe_{2-x}Al_xO_4$ (with $x = 0.0$ and 1.0) single-phase nanopowders are shown in Fig 4a, b. The particles of both samples are approximately spherical in shape, and their size distribution is uniform with the particle size in nanoscale. The particles size of the $CoFe_2O_4$ sample is mostly in the size range of 65–75 nm, larger than average crystallite size estimated from XRD measurements. The reason for this discrepancy is that at $CoFe_2O_4$ sample each particle consists of more than one crystallite [25]. The particle size of the $CoFeAlO_4$ sample is in the size range of 9–10 nm in good agreement with the average crystallite size determined from the XRD analysis. This means that at $CoFeAlO_4$ sample, most of the particles are single crystallite.

Figure 5a–d shows the SEM images of the $CoFe_2O_4$ nanoparticles calcined at 800 °C, $CoFe_{0.5}Al_{1.5}O_4$ nanoparticles calcined at 1000 and 1100 °C and the histogram of their grain size distribution, respectively. As seen, $CoFe_2O_4$ nanoparticles are nearly spherical in shape. The grain size distribution histograms from sampling of about 130 particles from SEM micrographs are presented in Fig. 5d. The grain size values are distributed in a range of 25–165 nm and the average grain sizes estimated by statistical method is ∼77 nm in good agreement with TEM measurement. The grain sizes distribution histograms of $CoFe_{0.5}Al_{1.5}O_4$ samples calcinated at 1000 (1100) °C reveal that the grain sizes of samples are distributed in a range of 60–180 (115–265) nm. For these samples, with increasing calcination temperature, the average grain size dramatically increases. The average grain size is evaluated to be about 91 and 166 nm for samples calcined at 1000 and 1100 °C, respectively.

3.3.1 UV–Visible Spectroscopic Studies

UV–visible spectroscopic data has been analyzed to obtain the absorption coefficient (α) and optical band gap (E_g)

Content courtesy of Springer Nature, terms of use apply. Rights reserved.

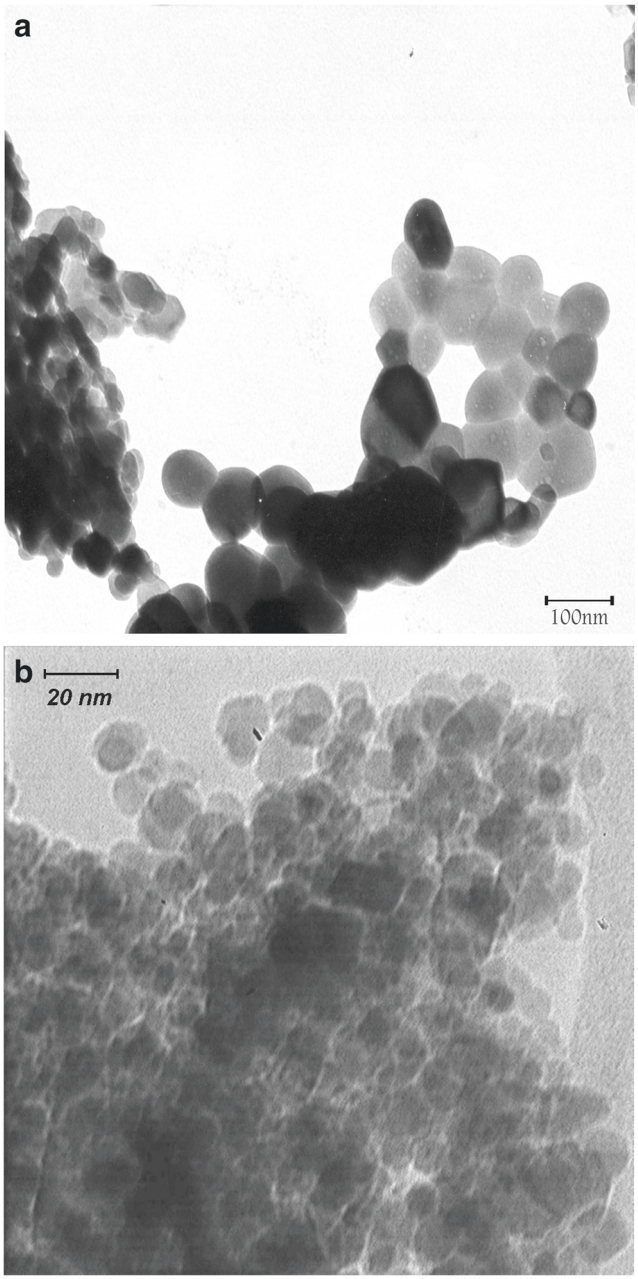

Fig. 4 TEM bright field image of **a** $CoFe_2O_4$ and **b** $CoFeAlO_4$ ferrite powders

of the $CoFe_{2-x}Al_xO_4$ ($x = 0.0, 0.5$,and 1.0) nanoferrites. The absorption coefficient of the nanoparticles has been calculated using the fundamental relationships [26]:

$$\alpha = 2.303\frac{A}{D} \tag{5}$$

where A is the absorbance, and D is the average crystallites size of the sample [26]. In these calculations, the average crystallite sizes calculated by Scherrer's method were used.

For a direct band gap material, the absorption coefficient is also given by [27]:

$$(\alpha h\upsilon)^2 = c(h\upsilon - E_g) \tag{6}$$

where c is constant and $h\upsilon$ is energy of photon. The direct energy band gap (E_g) values were obtained by extrapolating the linear part of the $(\alpha h\upsilon)^2$ curve vs. photon energy ($h\upsilon$) as shown in Fig. 6

The estimated values of E_g are found to be about 5.1, 5.2, and 5.8 eV for sample with $x = 0, 0.5$, and 1.0, respectively. As seen, it increases with Al^{3+}concentration (x) which may be due to a decrease in the particle size. This can be explained on the basis of Bras effective mass model [26] where E_g can be expressed as a function of particle size as:

$$E_g = E_g^{bulk} + \frac{\hbar^2\pi^2}{2eD^2}\left(\frac{1}{m_e} + \frac{1}{m_h}\right) - \frac{1.8e^2}{4\pi\varepsilon D\varepsilon_\circ} \tag{7}$$

where E_g^{bulk} is the bulk energy gap, D is the particle size, m_e (m_h) is the effective mass of electrons (holes), ε is the relative permittivity, ε_0 is the permittivity of free space, $\hbar$ is the Planck's constant divided by 2π, and e is the charge on electron.

3.4 Magnetic Properties

The room temperature magnetization hysteresis loops $M(H)$ of $CoFe_{2-x}Al_xO_4$ ($x = 0.0, 0.5, 1.0$, and 1.5) samples calcined at 800 °C and of $CoFe_{0.5}Al_{1.5}O_4$ calcined at 800, 900, 1000, and 1100 °C are shown in Fig. 7a, b. The results including the saturation magnetization (M_s), coercivity (H_c), and anisotropy constant (K) are summarized in Table 2.

As seen, M_s, H_c, and K decrease with increasing Al^{+3} content. The substitution of non-magnetic Al^{+3} ions for Fe^{+3} ions, on the octahedral sites, decreases superexchange interaction between the tetrahedral (A) and octahedral [B] sites in spinel structure. It also decreases the magnetic moment of [B] site and hence magnetization because the net magnetic moment of the lattice is given by difference of the magnetic moments of sublattices A (M_A) and B (M_B), $M_B - M_A$ [7, 13, 28]. These are why the M_s decreases with increase of Al concentration. On the other hand, the crystallite size and surface effects may be the other reasons for decrease in magnetization [28, 29]. The measured magnetization M_s for $CoFe_2O_4$ nanopowders was found to be $\tilde{6}1$ emu/g, which is lower than that of the bulk cobalt ferrite (80 emu/g [30]). This may be due to the fact that for smaller particles, the surface to volume ratio is higher as the spin disorder effects and canting of surface spin caused by broken exchange bonds on the surface lead to a decrease in magnetization [13]. The saturation magnetization of sample $x = 0.5$ is approximately equal to that of $x = 0$. Since Al^{3+}

Content courtesy of Springer Nature, terms of use apply. Rights reserved.

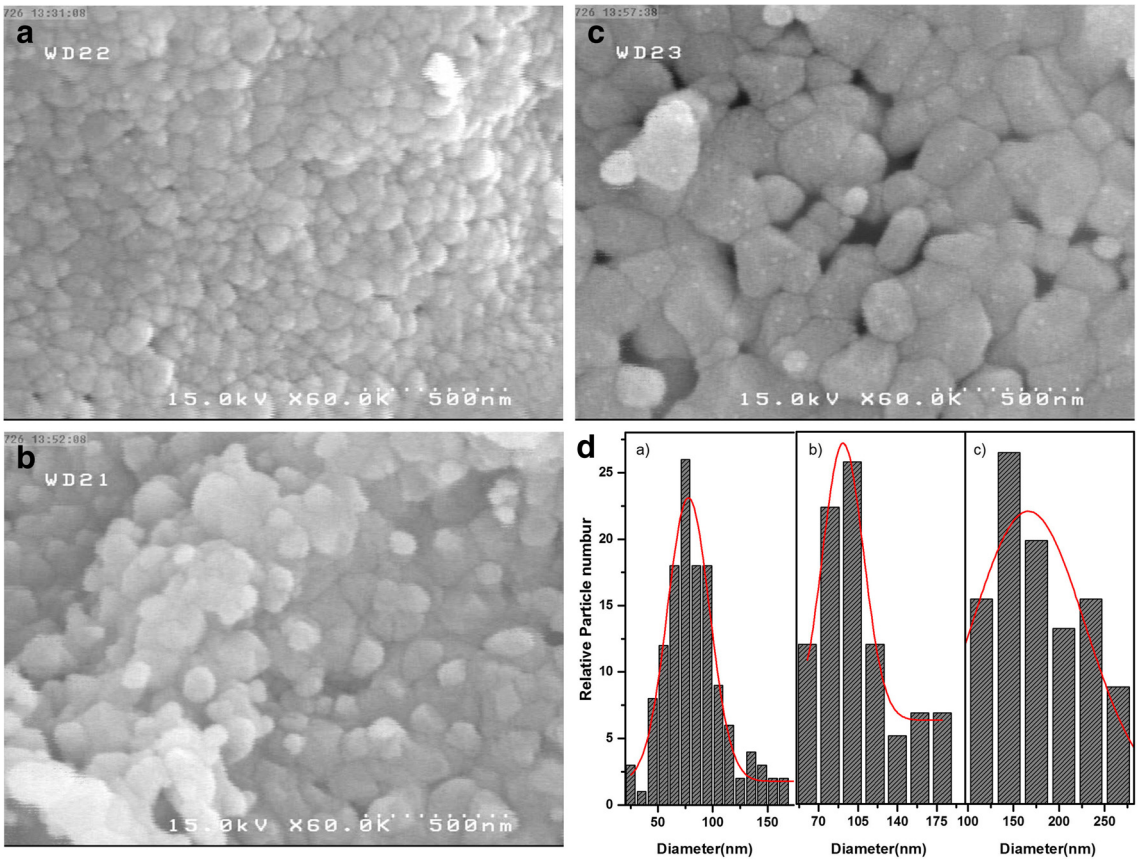

Fig. 5 SEM images of **a** $CoFe_2O_4$, **b** $CoFe_{0.5}Al_{1.5}O_4$ sample calcinated at 1000 °C, **c** $CoFe_{0.5}Al_{1.5}O_4$ sample calcinated at 1100 °C, and **d** histogram of their grain size distribution obtained by statistical method

ions do not have any strong preference for (A) or [B] sites in the cobalt ferrite [31], initially they substitute into both (A) and [B] sites in approximately equal numbers as Fe^{+3} ions are distributed in both (A) and [B] sites. Thus, the magnetic moments of M_A and M_B are reduced approximately in equal amounts as the saturation magnetization is remained almost unchanged. By further substitution of Al for Fe ($x > 0.5$), the saturation magnetization decreases because more non-magnetic ions are substituted at the expense of magnetic Fe ions. Moreover, because of its non-magnetic nature, there would be no superexchange interaction between Co/Fe and Al ions. Thus, with increasing Al content, the number of superexchange interactions and hence magnetization decrease.

It can be seen from Table 2 that the saturation magnetization, coercivity, and anisotropy constant values decrease with increase in calcination temperature. Reduction in the saturation magnetization with increasing calcination temperature from 800 to 900 °C can be attributed to decrease of crystallinity of Co_7Fe_3 phase. Decrease in saturation magnetization with increasing calcination temperature from 1000 to 1100 °C may be due to the redistribution of cations between (A) and [B] sites, as explained before in Section 3.2. With substitution of Al^{+3}, which has strong preference for occupying the [B] sites [13], some of Co^{+2} ions migrate from [B] to (A) sites and hence decrease the concentration of cobalt ions in [B] sites. This reduces the magnetic moment of [B] site and also decreases net magnetic moments. The coercivity is related to saturation

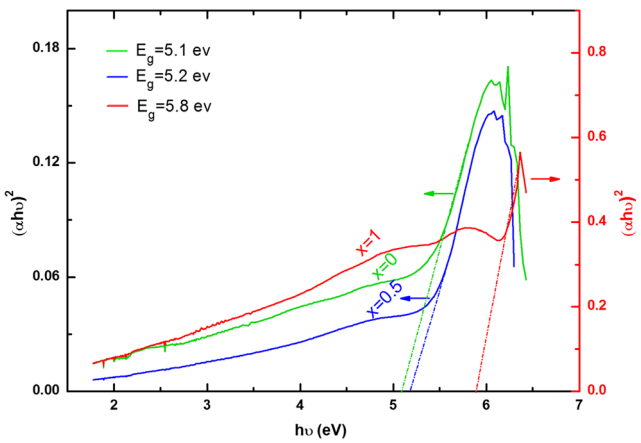

Fig. 6 Plots of $(\alpha h\upsilon)^2$ versus $h\upsilon$ for $CoFe_{2-x}Al_xO_4$ ($x = 0$, 0.5, and 1) nanoferrites calcinated at 800 °C

Content courtesy of Springer Nature, terms of use apply. Rights reserved.

Table 2 Parameters obtained from magnetic measurement of $CoFe_{2-x}Al_xO_4$ ($x = 0, 0.5, 1.0$, and 1.5) calcined at 800–1100 °C

x	$T_{calcination}$ (°C)	M_s (emu/gm)	H_c (Oe)	K (erg/gm)
0	800	61.25	1102	7.031×10^4
0.5	800	60.48	583	3.675×10^4
1	800	55.50	578	3.079×10^4
1.5	800	42.75	498	2.218×10^4
	900	41.06	450	1.923×10^4
	1000	3.99	265	1.10×10^3
	1100	1.52	79	1.25×102

magnetization and anisotropy constant by using the following relation [32]:

$$H_c = \frac{0.96K}{M_s} \tag{8}$$

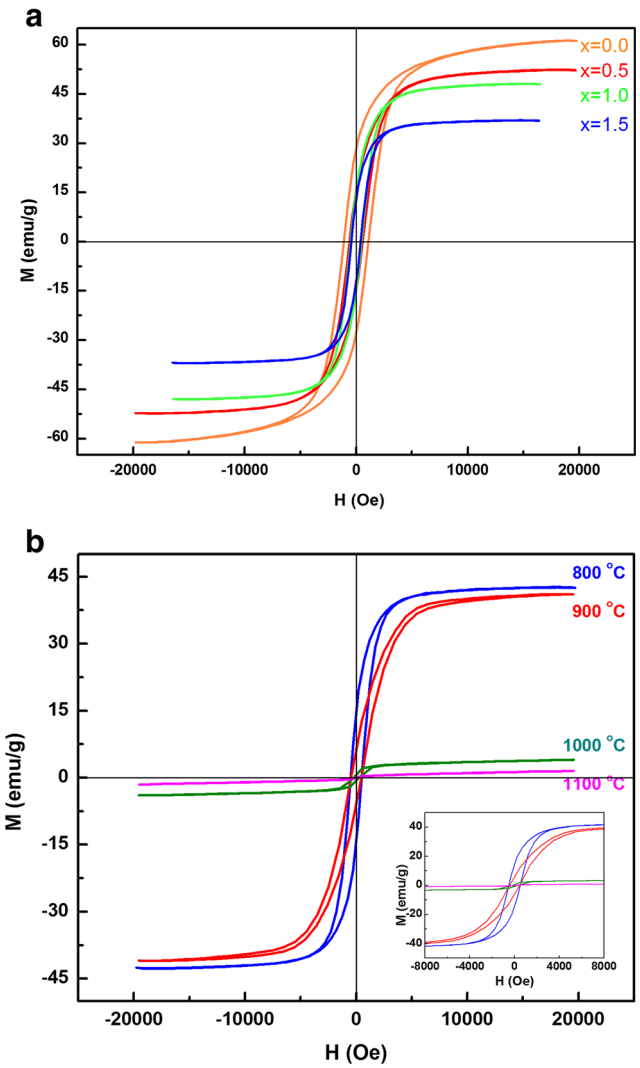

Fig. 7 Magnetic hysteresis loops at 27 °C for **a** samples $CoFe_{2-x}Al_xO_4$ ($x = 0.0, 0.5, 1.0$, and 1.5) calcinated at 800 °C and **b** $CoFe_{0.5}Al_{1.5}O_4$ powders calcinated at 800, 900, 1000, and 1100 °C. *Inset* shows the low field behavior for each case

As seen from Table 2, coercivity reduces with increasing Al concentration as well as increasing calcination temperature. This can be attributed to decrease in anisotropy constant K because of migration of Co ions from [B] sites reducing the spin–orbit coupling [23]. In fact, the strong and positive anisotropy of cobalt ferrite is primarily due to the presence of Co^{+2} ions on the [B] sites [23, 33]. So the crystal field is not capable of removing the orbital degeneracy of Co^{+2} at the [B] sites as the orbital magnetic moment is not quenched, and there is a strong spin–orbit coupling producing a large magnetocrystalline anisotropy energy in cobalt ferrite.

4 Conclusion

In this study, $CoFe_{2-x}Al_xO_4$ nanoparticles, where x is from 0 to 1.5 with a step of 0.5, have been prepared by sol–gel auto-combustion method, and subsequently, their structural, morphological, optical, and magnetic properties were investigated. XRD results show that $CoFe_{2-x}Al_xO_4$ ($x = 0, 0.5$, and 1) samples calcined at 800 °C and sample $CoFe_{0.5}Al_{1.5}O_4$ calcined at 1000 and 1100 °C have single-phase spinel structure. The values of lattice parameter, particle size, and unit cell volume decrease with increase of Al concentration, while the energy band gap increases possibly due to a decrease in particle size. For sample with $x = 1.5$, with increasing calcination temperature from 1000 to 1100 °C, the particle size, and crystallinity increase, the lattice parameter decreases. The room temperature magnetic measurements show the saturation magnetization, coercivity, and anisotropy constants decrease with Al concentration arising from the non-magnetic nature of Al^{3+} as well as decrease in the number of superexchange interactions. A decrease in coercivity and magnetization, with increasing calcination temperature from 1000 to 1100 °C, was also observed. This can be attributed to the cation redistribution between the tetrahedral and octahedral sites.

Acknowledgments The authors would like also to thank the "Iranian Nanotechnology Initiative Council" for their financial support.

Content courtesy of Springer Nature, terms of use apply. Rights reserved.

References

1. Arabi, H., Ganjali, F.: Structural and magnetic properties of cobalt and manganese doped Ni-ferrite nanoparticles. J. Supercond. Nov. Magn. **26**(4), 1031–1035 (2013)
2. Atif, M., Hasanain, S.K., Nadeem, M.: Magnetization of sol–gel prepared zinc ferrite nanoparticles: effects of inversion and particle size. Solids. State. Commun. **138**, 416–421 (2006)
3. Kim, W.C., Lee, S.W., Kim, S.J., Yoon, S.H., Kim, C.S.: Magnetic properties of Y-, La-, Nd, Gd-, and Bi-doped ultra"ne $CoFe_2O_4$ spinel grown by using a sol gel method. J. Magn. Magn. Mater. **215–216**, 217–220 (2000)
4. Gul, I.H., Maqsood, A.: Structural, magnetic and electrical properties of cobalt ferrites prepared by the sol–gel route. J. Alloys Compd. **465**, 227–231 (2008)
5. Gharagozlou, M.: Synthesis, characterization and influence of calcination temperature on magnetic properties of nanocrystalline spinel Co–ferrite prepared by polymeric precursor method. J. Alloys Compd. **486**, 660–665 (2009)
6. Köseoğlu, Y., Oleiwi, M.I.O., Yilgin, R., Koçbay, A.N.: Effect of chromium addition on the structural,morphological and magnetic properties of nano-crystalline cobalt ferrite system. Ceram. Int. **38**, 6671–6676 (2012)
7. Aghav, P.S., Dhage, V.N., Mane, M.L., Shengule, D.R., Dorik, R.G., Jadhav, K.M.: Effect of aluminum substitution on the structural and magnetic properties of cobalt ferrite synthesized by sol–gel auto combustion process. Phys. B. **406**, 4350–4354 (2011)
8. Raghavender, A.T., Jadhav, K.M.: Dielectric properties of Al-substituted Co ferrite nanoparticles. Bull. Mater. Sci. **32**, 575–578 (2009)
9. Vlazan, P., Vasile, M.: Synthesis and characterization $CoFe_2O_4$ nanoparticles prepared by the hydrothermal method. J. Optoelectron. Adv. Mater. **4**, 1307–1309 (2010)
10. Ai, L., Jiang, J.: Influence of annealing temperature on the formation, microstructure and magnetic properties of spinel nanocrystalline cobalt ferrites. Curr. Appl. Phys. **10**, 284–288 (2010)
11. Raghavender, A.T., Pajic, D., Zadro, K., Milekovic, T., Rao, P.V., Jadhav, K.M., Ravinder, D.: Synthesis and magnetic properties of $NiFe_{2-x}Al_xO_4$ nanoparticles. J. Magn. Magn. Mater. **316**, 1–7 (2007)
12. Airimioaei, M., Ciomaga, C.E., Apostolescu, N., Leontie, L., Iordan, A.R., Mitoseriu, L.M.N.: Synthesis and functional properties of the $Ni_{1-x}MnxFe_2O_4$ ferrites. J. Alloys Compd. **509**, 8065–8072 (2011)
13. Mozaffari, M., Abooalizadeh, Z., Amighian, J.: Investigation of magnetic properties of Al substituted nickel ferrite nanopowders, synthesized by the sol–gel method. J. Magn. Magn. Mater. **323**, 2997–3000 (2011)
14. Song, S.H.: Magnetic and magnetoelastic properties of M-substituted cobalt ferrites (M = Mn, Cr, Ga, Ge). Iowa State University, PhD thesis (2007)
15. Chae, K.P., Lee, J.G., Kweon, H.S., Lee, Y.B.: The crystallographic, magnetic properties of Al, Ti doped $CoFe_2O_4$ powders grown by sol–gel method. J. Magn. Magn. Mater. **283**, 103–108 (2004)
16. Raghavender, A.T., Kulkarni, R.G., Jadhav, K.M.: Magnetic properties of mixed cobalt-aluminum ferrite nanoparticles. Chin. J. Phys. **48**, 512–522 (2010)
17. Srivastava, M., Chaubey, S., Ojha, A.K.: Investigation on size dependent structural and magnetic behavior of nickel ferrite nanoparticles prepared by sol–gel and hydrothermal methods. Mater. Chem. Phys. **118**, 174–180 (2009)
18. Nguyet, D.T.T., Duong, N.P., Hung, L.T., Hien, T.D., Satoh, T.: Crystallization and magnetic behavior of nanosized nickel ferrite prepared by citrate precursor method. J. Alloys Compd. **509**, 6621–6625 (2011)
19. Tian, X., Liu, X.D., Xu, J., Feng, H.W., Chi, B., Huang, L.H., Yan, S.F.: Microstructures and electrochemical characteristics of $Mm_{0.3}Ml_{0.7}Ni_{3.55}Co_{0.75}Mn_{0.4}Al_{0.3}$ hydrogen storage alloys prepared by mechanical alloying. Int. J. Hydrogen Energy **34**, 2295–2302 (2009)
20. Jacob, J., Abdul Khadar, M.: Investigation of mixed spinel structure of nanostructured nickel ferrite. J. Appl. Phys. **107**, 114310–114320 (2010)
21. Rebrov, E.V., Gao, P., Verhoeven, T.W.G., Schouten, J.C., Kleismit, R., Turgut, Z., Kozlowski, G.: Structural and magnetic properties of sol–gel $Co_{2x}Ni_{0.5-x}Zn_{0.5-x}Fe_2O_4$ thin films. J. Magn. Magn. Mater. **323**, 723–729 (2011)
22. Kumar, L., Kar, M.: Influence of Al^{+3} ion concentration on the crystal structure and magnetic anisotropy of nanocrystalline spinel cobalt ferrite. J. Magn. Magn. Mater. **323**, 2042–2048 (2011)
23. Al-Haj, M.: Microstructure characterization and magnetic behavior of $NiAl_xFe_{2-x}O_4$ and $Ni_{1-y}Mn_yAl_{0.2}Fe_{1.8}O_4$ ferrites. J. Magn. Magn. Mater. **311**, 517–522 (2007)
24. Baykal, A.A., Kasapoglu, A., Durmus, Z., Kavas, H., Toprak, M.S., Koseoglu, Y.: CTAB-assisted hydrothermal synthesis and magnetic characterization of $Ni_xCo_{1-x}Fe_2O_4$ nanoparticles (x = 0.0, 0.6, 1.0). Turk. J. Chem. **33**, 33–45 (2009)
25. Bhukal, S., Namgyal, T., Mor, S., Bansal, S., Singhal, S.: Structural, electrical, optical and magnetic properties of chromium substituted Co–Zn nanoferrites $Co_{0.6}Zn_{0.4}Cr_xFe_{2-x}O_4$ ($0 \leq x \leq 1$) prepared via sol–gel auto-combustion method. J. Mol. Struct. **1012**, 162–167 (2012)
26. Zhu, H., Yang, D., Yu, G., Zhang, H., Yao, K.: A simple hydrothermal route for synthesizing SnO_2quantum dots. Nanotechnology **17**, 2386 (2006)
27. Farea, A.M.M., Kumar, S., Batoo, K.M., Yousef, A., Lee, C.G., Alimuddin.: Influence of the doping of Ti^{4+} ions on electrical and magnetic properties of $Mn_{1+x}Fe_{2-2x}Ti_xO_4$ ferrite. J. Alloys Compd. **469**, 451–457 (2009)
28. Shobana, M.K., Sankar, S.: structural, thermal and magnetic properties of $Ni_{1-x}Mn_xFe_2O_4$ nanoferrites. J. Magn. Magn. Mater. **321**, 2125–2128 (2009)
29. Shaikh, P.A., Kambale, R.C., Rao, A.V., Kolekar, Y.D.: Structural, magnetic and electrical properties of Co–Ni–Mn ferrites synthesized by co-precipitation method. J. Alloys Compd. **492**, 590–596 (2010)
30. Craik, D.J.: Magnetic Oxides, Part II, p. 703. Wiley, London (1975)
31. Sattar, A., EI-Sayed, H., EI-Shokroty, K., EI-Tabey, M.: Improvement of the Magnetic Properties of Mn-Ni-Zn Ferrite by the Non-magnetic Al3+-Ion Substitution. J. Appl. Sci **5**(1), 162–168 (2005)
32. Yang, H., Wang, Z., Song, L., Zhao, M., Wang, J., Luo, L.: A study on the coercivity and the magnetic anisotropy of the lithium ferrite nanocrystallite. J. Phys. D: Appl. Phys. **29**, 2574 (1996)
33. Melikhov, Y., Snyder, J.E., Jiles, D.C., Ring, A.P., Paulsen, J.A., Lo, C.C.H., Dennis, K.W.: Temperature dependence of magnetic anisotropy in Mn-substituted cobalt ferrite. J. Appl. Phys. **99**, 08R102 (2006)

Content courtesy of Springer Nature, terms of use apply. Rights reserved.

Terms and Conditions

Springer Nature journal content, brought to you courtesy of Springer Nature Customer Service Center GmbH (“Springer Nature”).
Springer Nature supports a reasonable amount of sharing of research papers by authors, subscribers and authorised users (“Users”), for small-scale personal, non-commercial use provided that all copyright, trade and service marks and other proprietary notices are maintained. By accessing, sharing, receiving or otherwise using the Springer Nature journal content you agree to these terms of use (“Terms”). For these purposes, Springer Nature considers academic use (by researchers and students) to be non-commercial.
These Terms are supplementary and will apply in addition to any applicable website terms and conditions, a relevant site licence or a personal subscription. These Terms will prevail over any conflict or ambiguity with regards to the relevant terms, a site licence or a personal subscription (to the extent of the conflict or ambiguity only). For Creative Commons-licensed articles, the terms of the Creative Commons license used will apply.
We collect and use personal data to provide access to the Springer Nature journal content. We may also use these personal data internally within ResearchGate and Springer Nature and as agreed share it, in an anonymised way, for purposes of tracking, analysis and reporting. We will not otherwise disclose your personal data outside the ResearchGate or the Springer Nature group of companies unless we have your permission as detailed in the Privacy Policy.
While Users may use the Springer Nature journal content for small scale, personal non-commercial use, it is important to note that Users may not:

1. use such content for the purpose of providing other users with access on a regular or large scale basis or as a means to circumvent access control;
2. use such content where to do so would be considered a criminal or statutory offence in any jurisdiction, or gives rise to civil liability, or is otherwise unlawful;
3. falsely or misleadingly imply or suggest endorsement, approval , sponsorship, or association unless explicitly agreed to by Springer Nature in writing;
4. use bots or other automated methods to access the content or redirect messages
5. override any security feature or exclusionary protocol; or
6. share the content in order to create substitute for Springer Nature products or services or a systematic database of Springer Nature journal content.

In line with the restriction against commercial use, Springer Nature does not permit the creation of a product or service that creates revenue, royalties, rent or income from our content or its inclusion as part of a paid for service or for other commercial gain. Springer Nature journal content cannot be used for inter-library loans and librarians may not upload Springer Nature journal content on a large scale into their, or any other, institutional repository.
These terms of use are reviewed regularly and may be amended at any time. Springer Nature is not obligated to publish any information or content on this website and may remove it or features or functionality at our sole discretion, at any time with or without notice. Springer Nature may revoke this licence to you at any time and remove access to any copies of the Springer Nature journal content which have been saved.
To the fullest extent permitted by law, Springer Nature makes no warranties, representations or guarantees to Users, either express or implied with respect to the Springer nature journal content and all parties disclaim and waive any implied warranties or warranties imposed by law, including merchantability or fitness for any particular purpose.
Please note that these rights do not automatically extend to content, data or other material published by Springer Nature that may be licensed from third parties.
If you would like to use or distribute our Springer Nature journal content to a wider audience or on a regular basis or in any other manner not expressly permitted by these Terms, please contact Springer Nature at

onlineservice@springernature.com